A NOVEL METHOD FOR ENHANCED NEEDLE LOCALIZATION USING ULTRASOUND-GUIDANCE

BIN DONG, ERIC SAVITSKY, AND STANLEY OSHER

Abstract. In this paper, we propose a novel and fast method to localize and track needles during image-guided interventions. Our proposed method is comprised of framework of needle detection and tracking in highly noisy ultrasound images via level set and PDE (partial differential equation) based methods. Major advantages of the method are: (1) efficiency, the entire numerical procedure can be finished in real-time: (2) robustness, insensitive to noise in the ultrasound images and: (3) flexibility, the motion of the needle can be as irregular as one wants. Our method will enhance the ability of medical care-providers to track and localize needles in relation to objects of interest during image-guided interventions.

1. Medical Background

Image guided interventions have become the standard of care for many surgical procedures. Optimal visualization of the object of interest and biopsy needle in ultrasound images requires the use of specialized biopsy needles and high cost, cart-based ultrasound units. The success of image guided interventions is dependent on anatomic knowledge, visualization, and precise tracking and control of the biopsy needle. A majority of medical care-providers utilize low resolution ultrasound units. In addition, many office-based or emergency department procedures are performed using generic (non-specialized) needles. Unfortunately, the quality of the imagery obtained by most ultrasound units does not allow for clear and concise visualization of a regular needle during many needle-based procedures. The inability to clearly see the tip of a needle in relation to the object of interest (e.g., a vein, artery, or mass) makes such image guided interventions less accurate.

In view of the inadequacy of ultrasound technology identifying inserted needles with desired resolution, a new and improved system for tracking such needles needs to be developed. A more accurate method for localizing the distal tip of inserted needles will greatly improve the efficacy and safety of ultrasound image-guided interventions. In this paper, we shall employ modern level set and PDE methods and fast numerical algorithms to solve the needle tracking problem for ultrasound images.

Key words and phrases. Ultrasound image, segmentation, active contour, Bregman iterations, tracking.

Bin Dong and Stanley Osher are with the Department of Mathematics, University of California Los Angeles, CA 90095 USA (e-mails: bdong@math.ucla.edu; sjo@math.ucla.edu).

Eric Savitsky is with Department of Emergency Medicine, University of California Los Angeles, BOX 951777, 924 Westwood Blvd, Ste 300, Los Angeles, CA 90095-1777 (e-mail: esavitsk@ucla.edu).

The rest of the paper is organized as follows. In Section 2, we shall lay down the fundamental mathematical model which is the core of solving our problem. In Section 3 we shall describe the complete schematic procedure of needle localization. Numerical experiments on ultrasound image frames will be given in Section 4 and concluding remarks will be given in Section 5.

2. Mathematical Model

We denote the video frames of ultrasound images as $I(x,t)$ with $0 \leq I(x,t) \leq 1$, and define the integrated difference of frames as

$$f(x) := \int \big|G_\sigma(x) * \partial_t I(x,t)\big| dt, \tag{2.1}$$

where G_σ is Gaussian with standard deviation σ. If the motions of the needle, e.g. jiggling or insertion, are different from the motions of the tissues and organs, which is usually the case, then in $f(x)$ we can see regions with such motions highlighted. However these regions in $f(x)$ are usually not very clear and have noisy boundaries. Therefore, a robust and efficient segmentation on $f(x)$ is needed.

There are numerous image segmentation methods in the literature [1, 5, 6, 7, 8, 9]. Since the image $f(x)$ defined in (2.1) is close to binary, we consider the following energy introduced in [1]

$$E(u) = \int g(x)|\nabla u(x)|dx + \lambda \int |u(x) - f(x)|dx. \tag{2.2}$$

It is shown in [1] that for any minimizer u of (2.2) and for almost all threshold $\mu \in [0,1]$, the characteristic function

$$\mathbf{1}_{\Omega(\mu)=\{x:u(x)>\mu\}}(x)$$

is a *global minimizer* of the corresponding geometric active contour model (see [1] for more details). Therefore, a segmentation of $f(x)$ can be obtained by first computing a minimizer of (2.2) and then letting $\Omega := \{x : u(x) > 0.5\}$. Now the key issue here is to minimize (2.2) efficiently.

To minimize the energy (2.2) efficiently, we adopt the idea of the split Bregman method introduced in [2]. Define

$$|d|_* := g(x)\sqrt{d_1^2 + d_2^2} + \lambda|d_3| \quad \text{and} \quad Fu := (\nabla u^T, u - f)^T,$$

then minimizing energy (2.2) is equivalent to

$$\begin{aligned} \text{Minimize} \quad & \int |d|_* \\ \text{s.t.} \quad & d = Fu. \end{aligned} \tag{2.3}$$

After "Bregmanizing" the constrained optimization problem (2.3), we obtain the following algorithm which minimizes the original energy (2.2) rather efficiently (the derivation is similar to that in [2]),

$$\begin{aligned} (u^{k+1}, d^{k+1}) &= \text{argmin}_{u,d} \int |d|_* + \frac{\mu}{2}\|d - Fu - b^k\|_2^2 \\ b^{k+1} &= b^k + \big(Fu^{k+1} - d^{k+1}\big). \end{aligned} \tag{2.4}$$

For convenience, we denote $\bar{d} = (d_1, d_2)^T$ and hence $d = (\bar{d}, d_3)^T$. Similarly, we can define $\bar{b}$ and b. Then we introduce the following algorithm to solve (2.4):

Algorithm 1. We start with $d^0 = \mathbf{0}$ and $b^0 = \mathbf{0}$.

(1) First update u by solving

$$(-\Delta + I)u^{k+1} = \nabla \cdot (\bar{b}^k - \bar{d}^k) + d_3^k + f - b_3^k;$$

(2) Then update d by

$$d_1^{k+1} = \max(s^k - \frac{g(x)}{\mu}, 0) \cdot \frac{u_x^k + b_1^k}{s^k},$$
$$d_2^{k+1} = \max(s^k - \frac{g(x)}{\mu}, 0) \cdot \frac{u_y^k + b_2^k}{s^k},$$
$$d_3^{k+1} = \text{shrink}(u^k - f + b_3^k, \frac{\lambda}{\mu}),$$

where $s^k = |\nabla u^k + \bar{b}^k|$.

(3) Finally update b^{k+1} by

$$b^{k+1} = b^k + \big(F(u^{k+1}) - d^{k+1}\big);$$

(4) If $\frac{\|u^{k+1} - u^k\|}{\|u^k\|} > \text{tol}$, go back to step 1 and repeat.

The Algorithm 1 is very efficient in terms of total number of iterations and the cost for each iteration. According to our experiments, it usually only takes about 30 iterations until $\frac{\|u^{k+1} - u^k\|}{\|u^k\|} \approx 10^{-3}$. For each iteration in Algorithm 1, the major calculation is in step 1, where the PDE can be solved rather efficiently by either FFT, for periodic boundary condition, or multigrid method, for Neumann and Dirichlet boundary conditions. An example is given in the following Figure 1 where noise was added to the original image. We note that the image is provided by Laboratory of Neural Imaging, Center for Computational Biology, UCLA.

For the special image $f(x)$ obtained from frames of ultrasound images by (2.1), the object of interest in $f(x)$ is either a needle or the tip of the needle, which are both simple geometric objects. Therefore, we can stop our iteration at an even earlier stage (e.g. in our experiments, we only perform two iterations) and the segmentation results would not change much if more iterations were carried out. The efficiency of Algorithm 1 ensures that the entire needle localization procedure can be finished in real-time. To be precise, by "real-time" we mean that the total time spent by the entire numerical procedure is no greater than that spent by the ultrasound machine in acquiring each image frame. A detailed description of the needle localization procedure will be given in next section.

3. Schematic Descriptions of Needle Detection and Tracking Procedure

The entire needle localization procedure can be decomposed into two phases. The first phase is to locate the needle in the images at the very beginning, based on a few seconds' image frames. During this phase, one can jiggle the needle or gently poke the tissues to help our algorithm locate the needle fast and accurately. The second phase is to track the motion of the tip of the needle when it moves.

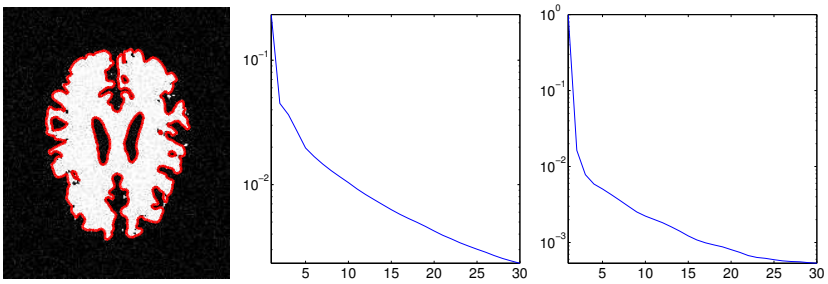

FIGURE 1. The left figure shows segmentation result using Algorithm 1; the middle one is the decay of $\frac{\|d-Fu^k\|}{\|d\|}$; and the right one is the decay of $\frac{\|u^{k+1}-u^k\|}{\|u^k\|}$.

3.1. **Phase I.** To locate the needle when it is first inserted into the tissue, we perform the following operations:

(1) Obtain $f(x)$ using (2.1) based on the previous 1-2 seconds' frames, denoted as $I(x,t)$;
(2) Segment the regions using (2.4) via the Algorithm 1 (with 2 iterations);
(3) Regularize the region obtained by step 2 via the fast algorithm of area-preserving mean curvature motion in [3, 4];
(4) Obtain the skeleton of the regularized region which represents the needle, and then the tip of the needle can be located.

To help localize the needle based on $f(x)$, one could gently jiggle the needle, in order to differentiate its motion from that of the tissues or organs. The following Figure 2 illustrates the four steps described above. We first note that it is obviously crucial to consider $f(x)$ instead of any single frame in order to rule out other regions with comparable intensities as the needle (e.g. some tissues or organs). The left two figures in Figure 3 show that if we perform segmentation directly on a single frame, we will capture several regions besides the needle. We also note that the third step above is important because otherwise, we may not get a single line representing the needle, but several branches (see the right figure in Figure 3). In step 4, there is always an ambiguity of the tip (it could be the alternative end of the line). However the ambiguity can be easily removed whenever the needle starts moving. Therefore, here and in the experiments below, we assume the tip is picked up correctly.

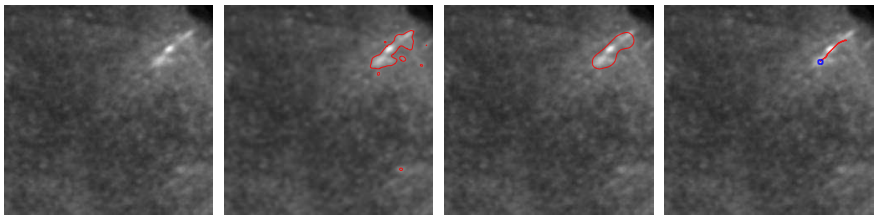

FIGURE 2. The four figures from left to right describes the four steps, and the four images are the same one $f(x)$ obtained by (2.1).

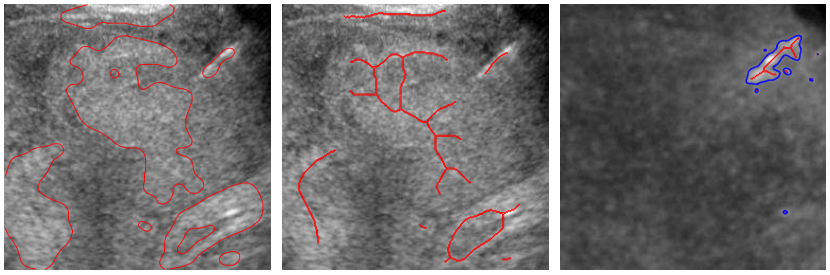

FIGURE 3. Left figure shows direct segmentation of one single frame; middle one shows the skeletons extracted from the segmented regions; right one shows the importance of step 3 in Phase I, where the blue curve is represented by the solution u obtained form step 2, and the red one is the skeleton by step 4.

3.2. **Phase II.** The second phase is to track the movements of the tip of the needle starting from the location we obtained from Phase I. We perform the following operations:

(1) Obtain $f(x)$ using (2.1) based on the current and the previous 1-2 frames;
(2) Segment the regions using (2.4) via the Algorithm 1 (with 2 iterations);
(3) Regularize the region obtained by step 2 via the fast algorithm of area-preserving mean curvature motion in [3, 4];
(4) Shrink the region, which possibly has disconnected components, to points and then choose one point from the set of points that is closest to the previous tracked location.

The following Figure 4 illustrates the four steps described above. We note that when the noise level is high or some irregular motions exist in tissues or organs, multiple locations may be captured in step 3, most of which are false detections. Therefore, step 4 affects the smoothness of the overall tracking. Evidently, we can use other ways to estimate the tip of needle based on the multiple locations captured in step 3. For example, if we know a priori that the needle moves in a regular fashion, then we can estimate the location of the tip based on the current multiple choices and the previously chosen locations such that the overall motion curve is smooth. For our experiments in Section 4, we only use the simpler operation described in step 4 because the needle moves in an irregular fashion. However, the result of the overall tracking is still quite satisfactory. We also note that in step 1, instead of considering the entire image $f(x)$, we can just consider a patch of $f(x)$ that centered at the previously located point (location of the tip in the previous frame). In this way, we can save some computations and also increase the smoothness of the overall tracking. Again, this only works when the motion of the needle is not too fast. For this reason, we will still use the entire image $f(x)$ in our experiments in Section 4.

4. NUMERICAL RESULT

All of the frames of ultrasound images are obtained by a Sonosite (Titan) ultrasound machine. The ultrasound machine captures 20 frames per second. In our following experiments, 120 frames are used, including 20 frames in Phase I and 100

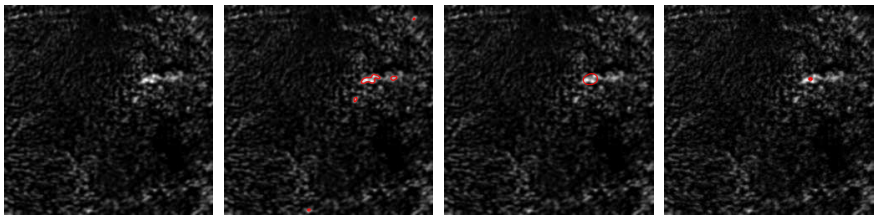

FIGURE 4. The four figures from left to right describes the four steps.

frames in Phase II. Each image is of size 251×251. In Figure 5 we present 5 of the 20 frames in Phase I, and in Figure 7 we present 12 of the 100 frames in Phase II.

The numerical results for Phase I are given in Figure 6, and those for Phase II are given in Figure 8. We note that the PDE in (1) of Algorithm 1 is solved by FFT. Here we also provide a ground truth in Figure 9 as validation of our results, where we manually selected the positions of the needle based on neighboring frames. We note that for almost all of the frames during Phase II, the tracking is rather accurate. However for some of the frames, the localization is not very accurate, for example the fourth figure in the first row of Figure 8. The reason is because of acoustic shadows in some image frames, which appear in $f(x)$ with high intensities and conceal the movement of the tip of the needle (see the middle figure of Figure 10). However, an acoustic shadow only seems to appear in $f(x)$ occasionally when we extract the needle, instead of inserting the needle, and an accurate tracking of the needle is only required during insertion. Therefore in practice, this error is not an issue and will not affect the safety concerns during image guided surgical operations.

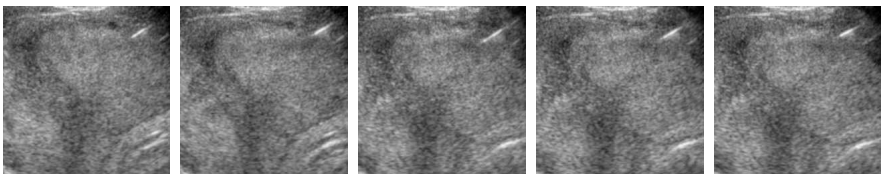

FIGURE 5. Images from left to right are 5 sample frames among total 20 frames of ultrasound images during Phase I.

5. Conclusion

Image guided interventions have become the standard of care for many surgical procedures. One of the most important problems in image guided interventions for ultrasound images is the precise tracking and control of biopsy needles. In this paper, we introduced a novel and efficient method for needle localization in highly noisy ultrasound images. Our numerical experiments showed that our proposed method tracks the tip of needle efficiently with excellent accuracy.

Acknowledgements

We would like to thank Jyotsna Vitale from the Radiology Department of UCLA for providing the ultrasound data. The research is supported by SN-30014, Center

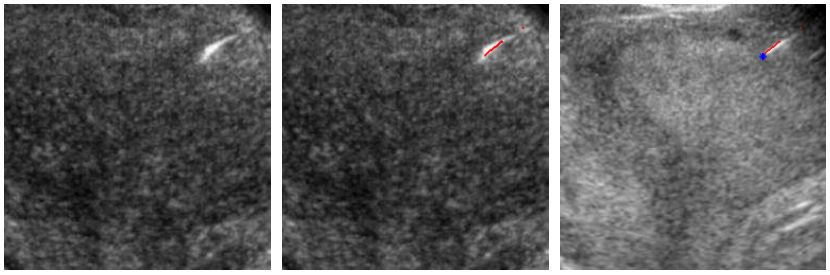

FIGURE 6. Left figure is $f(x)$ obtained from the 20 frames; middle one shows the result of localization of the body of the needle; right one shows the result of localization on the first image frame in Figure 5, where the blue dot indicates the tip of the needle.

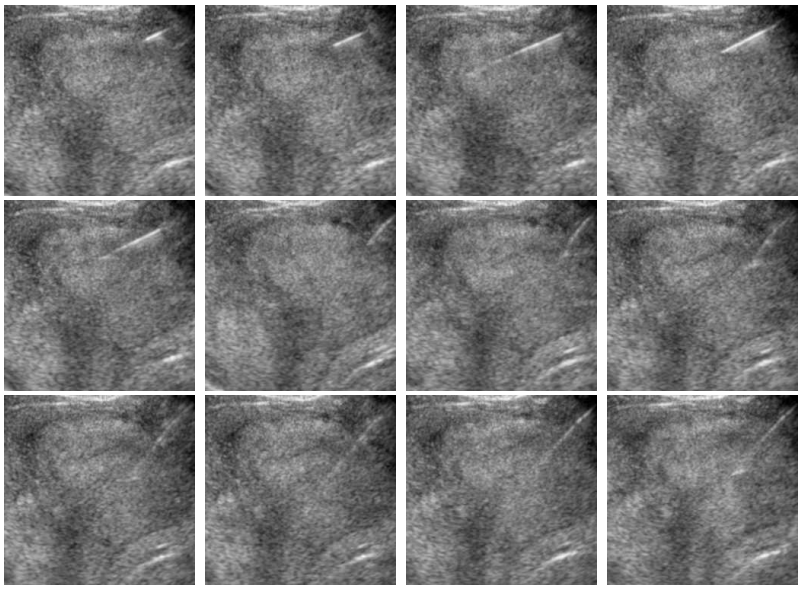

FIGURE 7. Images above are 12 sample frames among total 100 frames of ultrasound images during Phase II.

for Computational Biology NIH Toga; and the Telemedicine and Advanced Technology Research Center (TATRC) of the US Army Medical Research and Material Command (MRMC).

REFERENCES

1. X. Bresson, S. Esedoglu, P. Vandergheynst, J. Thiran and S. Osher, *Fast Global Minimization of the Active Contour/Snake Model*, Journal of Mathematical Imaging and Vision, 2007.
2. Tom Goldstein and Stanley Osher, *The Split Bregman Algorithm for L1 Regularized Problems*, CAM-Report **08-29**, April 2008.
3. B. Merriman, J. Bence and S. Osher, *Motion of multiple junctions, a level set approach*, J. Comput Phys, Vol. **112**, 334–363, 1994.
4. S. Ruuth and B. Wetton, *A simple scheme for volume preserving motion by mean curvature*, J. Sci Comput, vol. **19**, pp. 373–384, 2003.

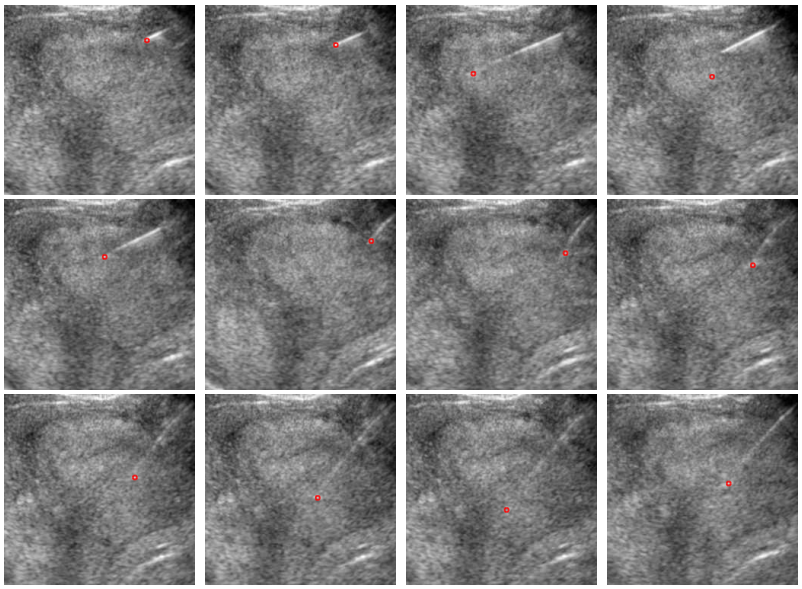

FIGURE 8. Tracking results of the 12 sample frames in Phase II shown in Figure 7.

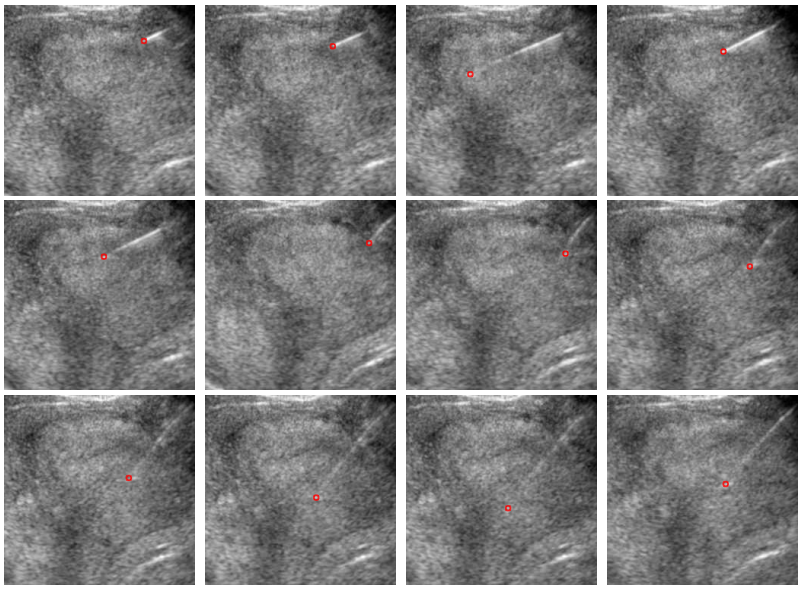

FIGURE 9. Manual segmentation results of the 12 sample frames in Phase II shown in Figure 7.

5. M. Kass, A. Witkin and D. Terzopoulos, *Snakes: Active Contour Models*, International Journal of Computer Vision, pp. 321–331, 1987.
6. V. Caselles, R. Kimmel and G. Sapiro, *Geodesic Active Contours*, International Journal of Computer Vision, Vol. **22(1)**, pp. 61–79, 1997.

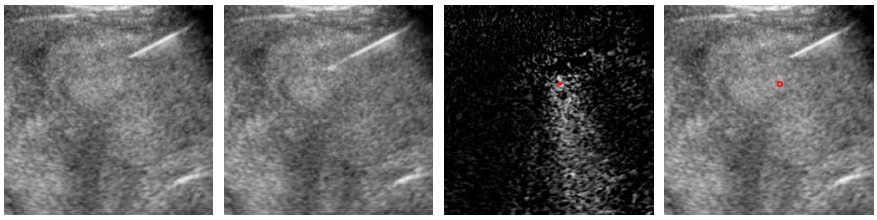

FIGURE 10. First figure is the current frame as shown in the fourth figure in first row of Figure 7; second figure is the previous frame of the first figure; third figure shows the corresponding $f(x)$ obtained from the first two figures and the red dot is the tracking result; the last one shows the tracking result on the current frame which is the same figure as in the upper fight figure of Figure 8.

7. S. Osher and R. Fedkiw, *Level Set Methods and Dynamic Implicit Surfaces*. Springer-Verlag, New York, 2003.
8. T. Chan and L. Vese, *Active Contours Without Edges*, IEEE Transactions on Image Processing, Vol. **10(2)**, pp. 266–277, 2001.
9. T. F. Chan, S. Esedoglu and M. Nikolova, *Algorithms for finding global minimizers of denoising and segmentation models*, SIAM J. Appl. Math. Vol. **66**, pp. 1632–1648, 2006.